J Nanopart Res (2017) 19: 291
DOI 10.1007/s11051-017-3995-3

TECHNOLOGY AND APPLICATION

Single Particle Extinction and Scattering allows novel optical characterization of aerosols

Federico Mariani · Vera Bernardoni · Francesco Riccobono · Roberta Vecchi · Gianluigi Valli · Tiziano Sanvito · Bruno Paroli · Alberto Pullia · Marco A. C. Potenza

Received: 11 May 2017 / Accepted: 7 August 2017 / Published online: 17 August 2017

Abstract We apply to aerosols the optical method of Single Particle Extinction and Scattering recently proposed for characterizing liquid suspensions and specifically adapted to the aim. It provides simultaneous measurements of the real and imaginary parts of the field scattered in the forward direction by single airborne particles passing through a tightly focused laser beam. The intensity of transmitted light is collected in the forward direction, thus realizing a self-reference interferometric scheme relying on the fundamentals of the optical theorem. A high frequency (20 MS/s), extended dynamics (12 bits) sampling is performed by a cheap segmented photodiode, and a specific pulse shape analysis is exploited to validate the signals against a precise mathematical model. We show that accessing two independent physical quantities allows to exploit physical models to recover the aerosol size distribution from the measurement of the refractive index, either real or even complex. Laboratory measurements have been performed with polydisperse aerosols made of water droplets and NaCl in the submicron range, and the system has been accurately characterized. Examples of measurements of graphite nanoparticles and Pyrethrum smoke are shown. Limitations are discussed.

Keywords Aerosol optical properties · Light scattering · Absorption · Extinction · Refractive index · Nano- and microparticles

F. Mariani · V. Bernardoni · R. Vecchi · G. Valli · T. Sanvito · B. Paroli · A. Pullia · M. A. C. Potenza (✉)
Department of Physics, Università degli Studi di Milano, via Celoria, 16, I-20133 Milan, Italy
e-mail: marco.potenza@unimi.it

V. Bernardoni · R. Vecchi · G. Valli · B. Paroli · A. Pullia · M. A. C. Potenza
INFN-Milan, via Celoria, 16, I-20133 Milan, Italy

F. Riccobono
Joint Research Centre, European Commission, via Fermi 2749, I-21027 Ispra, Italy

T. Sanvito
EOS s.r.l., viale Ortles 22/4, I-20139 Milan, Italy

M. A. C. Potenza
CIMAINA, Università degli Studi di Milano, via Celoria, 16, I-20133 Milan, Italy

Introduction

The knowledge of the light scattering and absorption properties of atmospheric aerosol is important for the assessment of aerosol effects both at local scale (e.g., visibility) and at global scale (i.e., the Earth's radiation balance). The main physical parameters allowing the description of light scattering and absorption by a particle are its complex refractive index, size, and shape (Bohren and Huffman 1983).

Gaining deeper insight into such parameters is of particular interest considering that the uncertainty currently associated to the aerosol-radiation interaction effect on the radiative forcing still ranges between − 0.77 and + 0.23 W/m^2 (IPCC 2013). Recently, Zarzana et al. (2014) have shown that very small variations (e.g.,

± 0.05) of the imaginary part of the refractive index for particles of about 150 nm in diameter leads to 20% variation in the modeled radiative forcing thus evidencing that refining input parameters for climate models is essential to reduce radiative forcing uncertainties.

To this aim, single-particle measurements of particle size and complex refractive index can be of particular interest: indeed, performing single-particle measurements allows deriving the physical properties of a particle ensemble (or to study particle subsets) straightforwardly. On the other hand, retrieving single-particle (or ensemble subset) properties starting from integrated measurements is an inversion problem that can be solved only using other constraints, if at all (e.g., Chemyakin et al. 2016).

Different approaches can be found in the literature to determine single-particle size and/or refractive index exploiting light-particle interaction. A widely used class of instruments determining particle size from the intensity of the scattered light at fixed angle is represented by optical particle counters (OPC; Heim et al. 2008; Sachweh et al. 1998) which work under the assumption that the measured particles are spherical and have the same refractive index of the material used for the calibration. Ongoing works are leading to more refined single-particle techniques providing both particle size in submicron range and refractive index: some of these single-particle techniques are based on particle trapping and thus they are more suitable to study the effects of evaporation, hygroscopic growth, or aging on the particle size and/or refractive index than for online monitoring of ambient aerosol. As examples, ultraviolet broadband light scattering (UV-BLS) was developed to determine the size and refractive index of non-absorbing particles down to few hundreds nanometer (David et al. 2016) from the intensity of scattered light at different wavelengths; Cotterell et al. (2015) developed and applied single-particle cavity ring-down spectroscopy (SP-CRDS) to determine single-particle extinction efficiency, as well as—thanks to tandem phase function measurements—particle size and refractive index. Recently, attention was given to the evaluation of the accuracy of the retrieved complex refractive index (Cotterell et al. 2016), reaching very high accuracy (< 0.1%) for particles with diameter in the range 1000–2000 nm and within 10% in the range 400–600 nm.

At the best of our knowledge, the only instrument developed with the aim of determining the complex refractive index of non-trapped single particles in air—thus specifically designed for online measurements—is a single-particle polar nephelometer (Nakagawa et al. 2016). In the current form, the instrument measures the scattering angular distributions in planes parallel and perpendicular to the polarization of the incident laser beam. The results were compared to simulations carried out by a priori assumptions on particles refractive index. Only in the case of nigrosine, an attempt to determine the complex refractive index of the material is performed by a minimization of squared residuals between measurements and predictions obtained at different refractive indices.

Here we describe a novel approach for the measurement of size and refractive index of aerosol in air based upon an optical layout which has been recently introduced and validated for liquid suspensions. It relies on the Single Particle Extinction and Scattering (SPES) method (Potenza et al. 2015a), allowing for the simultaneous measurement of the real and imaginary parts of the forward scattered field. The SPES method relies on a self-reference interferometric scheme in which particles are driven through the focal region of a light beam, and the transmitted light is collected onto a sensor placed in the far field; signal analysis further refines the instrument outputs, rejecting spurious signals. As well known (Bohren and Huffman 1983; Van de Hulst 1981), the field amplitude in the forward direction provides lot of information on the particle characteristics (optical theorem). Stemming from these concepts, SPES provides information of utmost interest—i.e., particle size and refractive index—under few or no assumptions (see "Single Particle Extinction and Scattering" section) (Potenza et al. 2015b; Villa et al. 2016), despite the extremely limited parameters measured (the real and imaginary parts of the adimensional scattering amplitude) (Potenza and Milani 2014).

Applying the SPES concept to measurements of aerosol in air as proposed in this work allows to do the following:

- Perform single-particle measurements of untreated samples. In this way, detailed statistics on the properties of the analyzed population can be obtained instead of the average properties obtained by integrated measurements; moreover, possible subsets of peculiar interest can be studied;
- Avoid any calibration: measurements of the scattering field are directly related to aerosol physical

parameters by the Mie theory in the spherical particle approximation;
- Reject spurious signals (e.g., due to the passage of more than a particle through the beam, or passages of particles out of the focal plane) through the analysis of signal characteristics;
- Determine both the particle size and the refractive index in the case of non-absorbing particles (in case of aerosol of homogeneous composition, size polydispersity allows to reach very high precision in the refractive index determination) (Potenza et al. 2015b);
- Determine, in case of absorbing particles:

  (a) The particle size and the imaginary part of the refractive index under assumptions on the real part of the refractive index
  or
  (b) The real and imaginary part of the refractive index if size segregation is performed upstream the SPES measurement cell (this approach has not been implemented yet);

- Gain information on non-spherical shape in case of aerosol of homogeneous composition: indeed, thanks to single particle detection, disagreement with results expected for spherical particles population can be identified (Potenza et al. 2016; Villa et al. 2016).

In this paper, we show the successful application of SPES to airborne particles in laboratory tests. Nevertheless, its characteristics can be exploited in the future by coupling with other instrumentation (e.g., a differential mobility particle sizer for size segregation) to complete the characterization of ambient aerosol.

In the following, we recall the fundamentals of the method, describe the experimental apparatus specifically designed to perform measurements in air, and discuss data analysis ("Single Particle Extinction and Scattering" section). In "Results" section, we report experimental results, including accurate measurements of submicron water droplets and NaCl particles, both produced by an atomizer (Topas aerosol generator ATM 220) and examples of SPES results obtained with graphite nanoparticles and pyrethrum smoke aerosols. Experimental results are the basis to discuss the advantages and limitations of the SPES method on the basis of experimental results. Finally, we discuss our conclusions and perspectives in "Discussion and conclusions" section.

Single Particle Extinction and Scattering

SPES method has been developed in the last years to operate with liquid suspensions of nano- and micron-sized particles. The fundamentals of the method, as well as a detailed, fully analytical description of the instrument response have been extensively given in Potenza et al. (2015a). A complete validation has been performed with very well-known particles of different materials suspended in water: spherical (Potenza et al. 2015b), non-spherical isometric (Potenza et al. 2015c), oblate and prolate (Villa et al. 2016), as well as dielectric and absorbing particles (Potenza et al. 2015a).

The method takes advantage from being absolutely calibration free. As mentioned above, thanks to the single particle detection, polydispersity is not an issue here. By contrast, relying on polydispersity, it is possible to assess with a high level of precision particle properties like refractive index (Potenza et al. 2015b) and shape (Villa et al. 2016).

The fundamentals of the method

We first define the dimensionless scattered amplitude $S(\theta)$ for a particle in a light beam of wave number $k = 2\pi/\lambda$ (where λ is the light wavelength). If A_0 is the complex amplitude of the illuminating field, the scattered amplitude $A(r,\theta)$ at distance $r = (x^2 + y^2 + z^2)^{1/2}$ and scattering angle θ (we assume azimuthal symmetry) is:

$$A(r,\theta) = S(\theta)\frac{\exp[-ikr + ikz]}{ikr}A_0 \quad (1)$$

Thanks to the extinction or optical theorem (OT) (Bohren and Huffman 1983; Mishchenko et al. 1999; Newton 1976; Van de Hulst 1981; Potenza et al. 2010), the *extinction* cross section C_{ext} (i.e., scattering (C_{sca}) + absorption (C_{abs}) cross sections) is simply related to the *forward scattered* amplitude $S(0)$:

$$C_{ext} = C_{sca} + C_{abs} = \frac{4\pi}{k^2}Re[S(0)] \quad (2)$$

Several methods have been conceived to measure $S(0)$: Michelson, Mach-Zender, and Smartt interferometers were

used to get rid of the intense transmitted beam, as accurately described in literature (Bassini et al. 1997; Batchelder and Taubenblatt 1989; Taubenblatt and Batchelder 1991). SPES method is much simpler. A single particle is sent along *x*-axis through the focal region of a light beam and both the transmitted (i.e., reference) and scattered waves are superimposed onto a sensor in the far field. When the particle is exactly on the optical axis (*z*-axis in Fig. 1), the two waves are perfectly concentric and interference is perfectly uniform. Accordingly to the OT, this is responsible for a depression of the reference beam intensity accounting for both the scattered and absorbed power, giving a rigorous measure of the extinction cross section C_{ext}. By contrast, when the particle is displaced along *x*-direction, waves are slightly skewed (see Fig. 1), skewness being imposed by the position of the particle. The intensity modulation imposed by interference is related to the modulus of the forward scattered field amplitude. Hence, the name of Single Particle Extinction and Scattering.

Interference between the (faint) scattered and the intense reference waves generates a small, time varying intensity modulation onto the sensor, a segmented quadrant photodiode (QPD) coupled with a custom front end electronics followed by an anti-aliasing, four poles Butterworth filter. Signals are then sent into synchronous analog to digital converters (ADC) and digitized data stored into a PC. Light intensity is sampled at a frequency much higher than the inverse transit time (see below), thus allowing a precise characterization of the intensity changes with time for each segment. A dedicated pulse shape analysis has been introduced in order to discard the events generated by particles out of the focal region, thanks to a rigorous validation method (Potenza et al. 2015a). Therefore, SPES results are intrinsically of high quality, with the drawback of a strong reduction in the overall number of selected particles which makes the measurement time increasing with respect to traditional OPCs.

Instrumental

Particles are sent at a speed of several meters per second through a Gaussian focal spot having a waist w_0 of some microns. Ideally speaking, the beam waist w_0 defines the sensitivity of the method, as it ultimately gives the section of the beam with respect to the cross section of the particle (see Potenza et al. 2015a). In this work, we report results obtained with $w_0 = 5.5$ μm. Care was posed to avoid any aberration, in any case limited to the spherical one thanks to the axial symmetry of the optical system. Therefore, signal durations of the order of approximately 5 μs are generated, sampled at a frequency of 20 MS/s, allowing to detect approximately 100 points for each photodiode quadrant for each event. An ultra-low noise laser (Coherent Ltd.; 5 mW power, 640 nm wavelength) has been adopted in order to limit the intrinsic, high frequency fluctuations. In fact, from a practical point of view, the laser fluctuations (about 10^{-3} for typical laboratory red lasers: see Sanvito et al. 2013) actually impose the main limitation to the sensitivity of the method; generally, they originate by

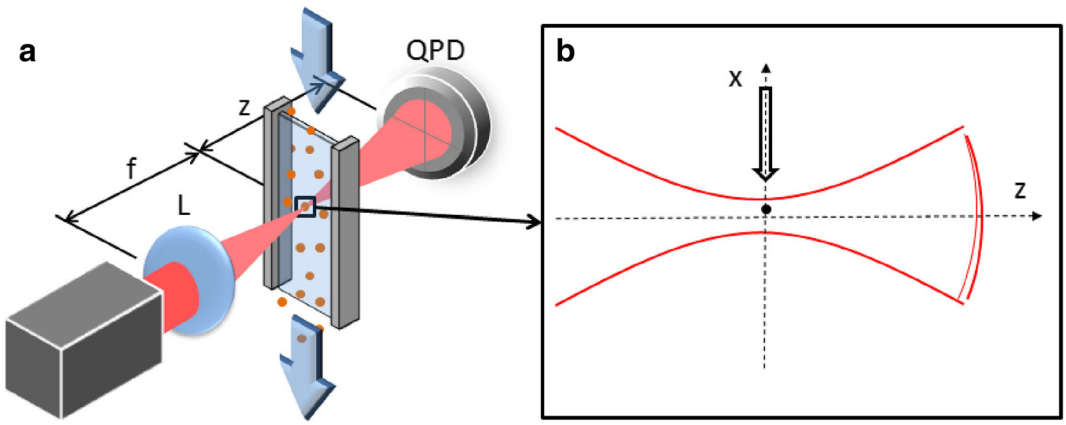

Fig. 1 Schematic of the SPES apparatus (**a**). A collimated laser beam is tightly focused by lens L with focal length *f* into the flow cell where particles are driven downward at constant speed. The emerging light is collected in the far field at a distance *z* by a quadrant photodiode (QPD). In **b**, we show the transmitted (thick line) and scattered (thin line) waves generated by a particle represented by the black dot. The interference of the transmitted and scattered spherical waves generates intensity fluctuations over the sensor

mode hopping into the crystal and therefore are very difficult to be avoided.

The front end electronics is specifically designed to provide two different outputs for each sensor:

(a) A fast signal, which provides a zero average signal proportional to the fast intensity fluctuations imposed by the particle passage through the beam;
(b) A slow signal obtained by applying a low pass filter with a time constant much longer than the transit time ($\tau = 250$ μs), for the continuous monitoring of the intensity of the beam onto the sensor.

This allows the continuous calibration of the signals to the reference beam power.

Furthermore, pulse shape analysis is exploited to remove spurious signals. A detailed description of the signal analysis can be found in Potenza et al. (2015a). It is noteworthy that pulse shape analysis allows to reject spurious events related to the passage of particles out of the focal plane as well as the possible passage of two particles through the beam.

As reported in Potenza et al. (2015a), thanks to the self-reference interference and the rigorous measurement of the beam power P, the signals can be analyzed without any adjustable parameter making the system absolutely calibration free. Notice that no other parameters are required, as λ and w_0 are well known for a given optical setup. This is a huge advantage of SPES method with respect to other instruments.

Data analysis: recovering the scattering amplitude

The knowledge of the forward scattered amplitude $S(0)$ carries a noticeable piece of information, although not enough to give the complete knowledge of the particle. As extensively discussed in Potenza and Milani (2014) and Potenza et al. (2015a), analyzing the 2D distribution of the measured $S(0)$ values from a collection of particles allows to give an estimate about refractive index (Potenza et al. 2015a). In that, a key role is played by the particle shape that, although giving a minimum effect thanks to the forward scattering geometry, still plays a role for aspect ratios larger than approximately 2–3 (Chylek et al. 1976; Villa et al. 2016). For almost spherical or even any isometric geometry, the refractive index can be measured with a precision better than 10%. If particles can be *assumed* to be spherical, much better accuracy is obtained from the average parameters obtained from a population of particles (Potenza et al. 2015b).

Under the common assumption of spherical particles, Mie theory allows building a table of complex values covering the $S(0)$ complex plane. For particles smaller than 1 μm and the case of pure dielectric, or even a negligible imaginary refractive index of the material, a one-to-one relation can be easily found between each point in the $S(0)$ plane and a given size-refractive index information. In Fig. 2, the look-up table (LUT) obtained for spherical, non-absorbing particles is shown in the complex plane: panel a shows the size in colors plotted in the complex plane and panel b shows the refractive index values (same axes). It is evident that if only one parameter is measured—i.e., information on extinction only or on scattering only is available as it usually occurs, e.g., using optical particle counters or extinction sensors (Ruth 2002; Sachweh et al. 1998)—an assumption on the particle refractive index is necessary for assessing the correct value for the size. Opposite, the SPES method performs two-parameter measurements allowing the contemporary knowledge of $Re\ S(0)$ (related to the extinction cross section) and $Im\ S(0)$ (related to the scattered intensity), thus allowing the contemporary retrieval of particle size and refractive index, overcoming limitations of traditional single particle measuring systems, which indeed are limited by the unknown refractive index.

The case of absorbing particles, i.e., non-negligible imaginary part of the complex refractive index, warrants a specific discussion. Particles endowed with absorption are described by at least three independent parameters (size, real, and imaginary parts of the refractive index), while with SPES we only access only two. Therefore, a rigorous inversion of the data is impossible even for spheres. Nevertheless, we stress that $S(0)$ is affected by absorption only for appreciable values of the imaginary part of the refractive index, e.g., higher than 0.1 approximately, as it can be easily derived from Mie calculations. Smaller values, although of interest for some applications in climate and radiative transfer problems (Albani et al. 2014; Bauer and Ganopolski 2014; Harvey 1988; Lambert et al. 2008), are actually invisible to SPES. Moreover, when dealing with appreciable absorption within the limits of the SPES method and by considering non-pathological values for the real part of the refractive indices of the materials typically encountered in aerosol science, the main role in determining the complex scattered amplitude is by far played by

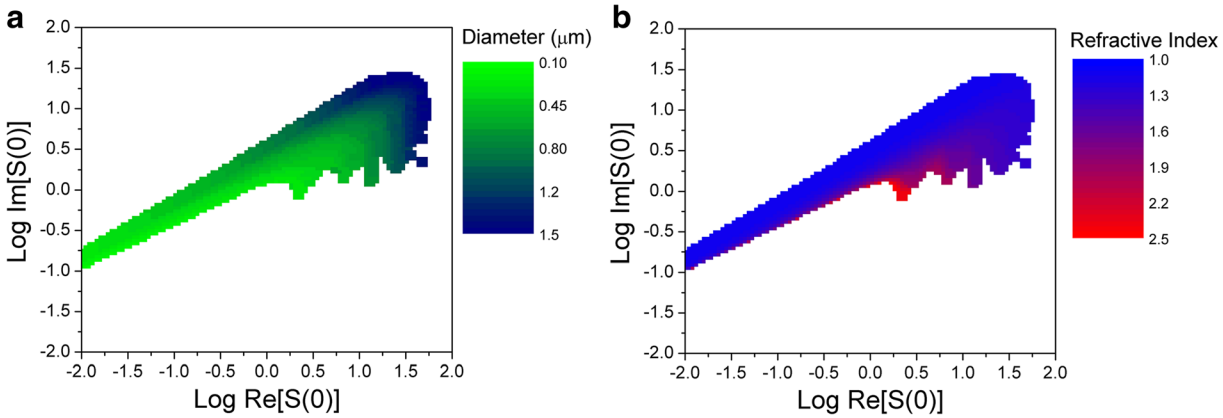

Fig. 2 The LUT obtained for dielectric spherical particles. **a** Size, **b** real part of the refractive index

the imaginary part. Therefore, from a practical point of view, the leading parameters characterizing the LUT will only be the particle size and imaginary part of the refractive index: the real part of the refractive can then be assumed to be fixed as a first approximation as it has only a minor influence on SPES results in this case. We stress that in many cases absorbing materials are not well described as homogeneous spheres, and the limitation imposed by fixing a given value for the real part of the refractive index is therefore negligible compared to the unconsidered effects of the non-spherical shape and/or internal structures (Sorensen 2001).

Alternatively, a different possible approach in analyzing SPES data can be used for a population of uniform particles, both for non-absorbing and absorbing materials. As already proven in the case of liquid-suspended particles (Potenza et al. 2015b), when a uniform composition can be assumed for all the measured particles, or even for a known subset of them, the measurement of the refractive index can be better obtained by finding the best value fitting the overall data set instead of considering the properties of single particles. In such a way, a much better determination of the refractive index is possible (both for the real and complex cases). Accuracy of a few percent can be reached. This means that the same results can then be used to recover a very precise particle size distribution, whose reliability certainly overcomes that of a traditional light scattering instrument, which assumes a priori a given refractive index (Potenza and Milani 2014). In this work, we applied this approach for both non-absorbing and absorbing particles. In the case of absorbing particles, we compared experimental data to a set of LUTs generated at different k values, thus obtaining the best estimate for the imaginary part of the refractive index of the entire population. Inversion has then been obtained by applying the corresponding LUT, thus associating each measured event to size and refractive index. In Fig. 3, we report the LUT obtained for absorbing spheres with an imaginary part of the refractive index $k = 0.2$, as we will exploit to interpret data below.

In the following section, we report about our experimental results obtained with different samples of particles with independent knowledge of some of the parameters giving rise to the scattered fields.

Results

In this section we report SPES data obtained on laboratory aerosols generated through a traditional atomizer (subsection A), graphite nanoparticles generated by a spark aerosol (subsection B), and smoke generated by a slow burning pyrethrum coil (subsection C).

We will show SPES data in two-dimensional (2D) plots of the complex scattered field. Histograms are represented, counting the number of measured events (validated particles) within each 2D bin in the plane. Numbers are normalized to the maximum value and represented in color scale: yellow = 0, blue = 1. We stress that, since the range of measured values is extended over decades, a log-log scale is mandatory. The only drawback is to hide the negative imaginary parts, since they have to be taken as positive and the sign considered separately, as we will discuss in detail later on.

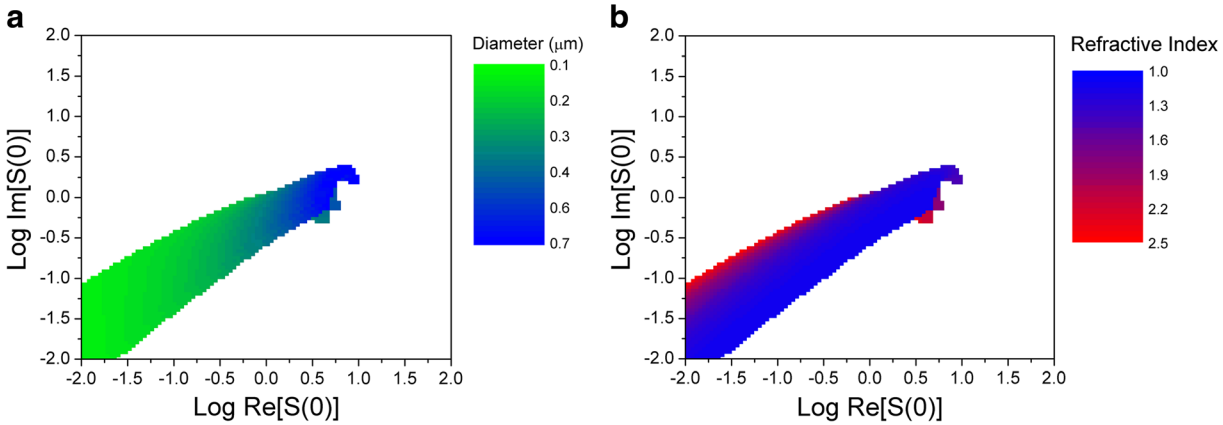

Fig. 3 The LUT obtained for absorbing spherical particles for an imaginary part of the refractive index $k = 0.2$. **a** Size, **b** real part of the refractive index

Aerosol generated by atomization

In order to validate the method with airborne particles, we performed a number of measurements in controlled laboratory conditions by means of an aerosol generator ATM 220 (Topas). It works as a two-substance nozzle based on the injection principle and is combined with a baffle placed close to the spray outlet. This integrated particle impaction section removes coarse spray droplets and results in a submicron particle size distribution. We compare results obtained by atomizing pure water and a saturated solution of NaCl in water. In both cases, we can easily exploit the Mie theory and the LUT described above for evaluating the particle size and refractive index, thanks to the spherical approximation. No absorption is considered here that can be easily proven to be negligible in our measurements. Raw data are shown in the complex plane with log-log axes as two-dimensional histograms.

In Figs. 4 and 5, we report the results obtained with pure water droplets. Data in Fig. 4 are those with positive imaginary part of $S(0)$, compared to the expected complex amplitudes obtained from the Mie theory (red line). Figure 5 represents the results exhibiting negative imaginary part of $S(0)$. We stress that the two populations have been collected simultaneously. No other selection has been used except the sign of the imaginary part.

Thanks to the precise knowledge of the refractive index of water and the spherical shape that can reasonably be assumed for the aerosol considered here, we can further analyze the data by considering the shape of the histogram in Fig. 4 at the highest absolute values of $Im\ S(0)$. We first notice that the data closely follow the expected behavior predicted by the Mie theory, characterized by a maximum in the imaginary values followed by a deep minimum due to the presence of the Mie oscillations (Van de Hulst 1981). Even more

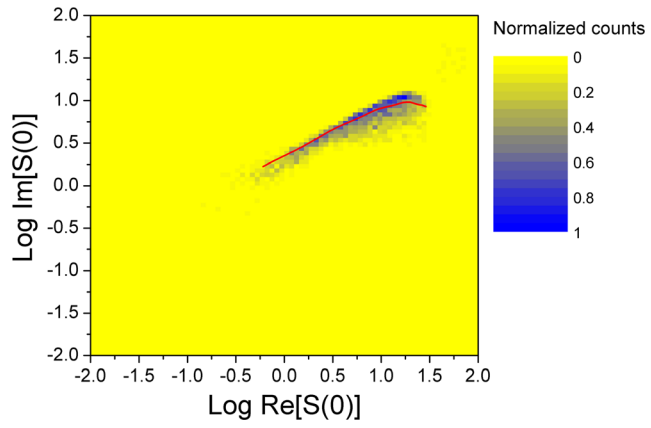

Fig. 4 Experimental results (color histogram) obtained with pure water droplets, compared to the expected values from the Mie theory (red line). Only data with positive imaginary parts of $S(0)$ are represented

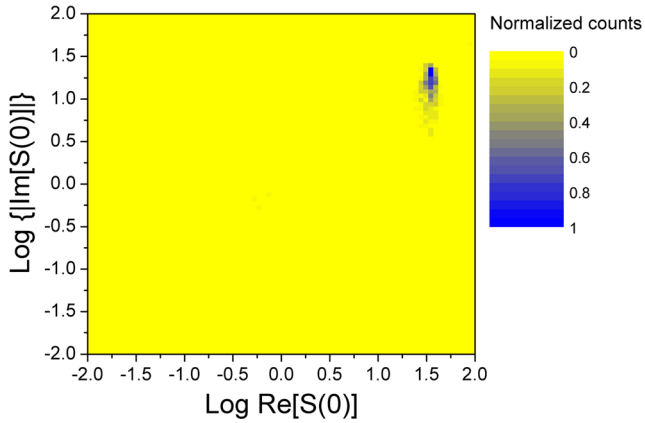

Fig. 5 Experimental results obtained with pure water droplets with negative imaginary parts. No other selection has been used except the sign of the imaginary part

interestingly, this region of the plot is expected to be characterized by the phase inversion of the scattered wave, namely the negative values of the imaginary parts of $S(0)$ observed in Fig. 5 where we show the data showing negative imaginary parts. As expected, the two populations are well separated. To our knowledge, this is the first time that this phase inversion has been clearly measured, thus supporting the reliability of the SPES approach.

Moreover, by means of the LUT discussed above, we have evaluated the size and refractive index of each particle. In Fig. 6, we show the results expressed as a

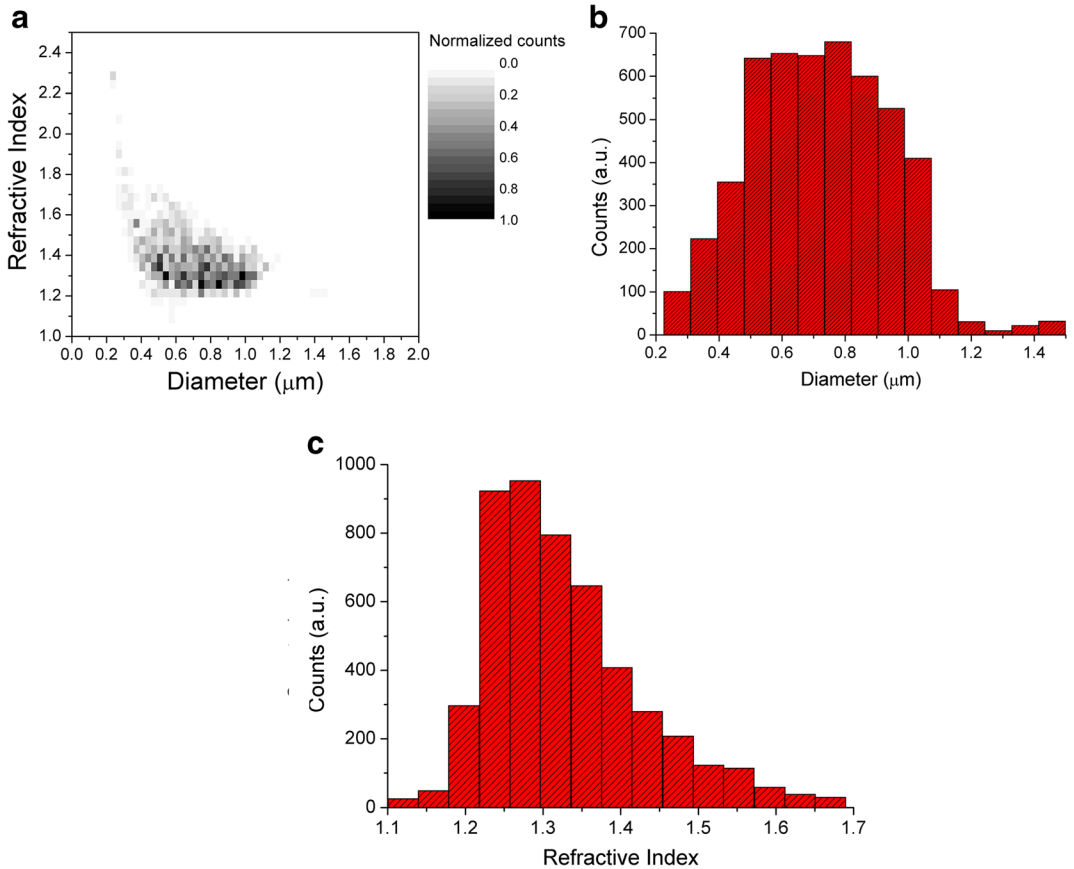

Fig. 6 **a** 2D plot of the number distribution of size (abscissas) and refractive index (ordinates) obtained from the data in Figs. 4 and 5 by means of the LUT represented in Fig. 2. In **b** and **c**, the size and refractive index distributions are reported

2D histogram as a function of diameter and refractive index (a), and the number distributions of diameters (b) and refractive indices (c). First of all, it is noteworthy that the particle size distribution has a sudden drop at about 500 nm radius, which is consistent with the aerodynamic size-cut performed by the aerosol generator. The average refractive index obtained from the histogram in Fig. 6b results $n = 1.32 \pm 0.1$, in agreement with the expected value for water, $n_w = 1.33$.

The same approach followed for pure water has been adopted for NaCl particles. The possibility to measure such particles is of particular interest because sea salt is the main natural source of aerosol on global scale. The corresponding results are plotted in Fig. 7, compared to the expected complex amplitudes calculated with the Mie theory for refractive index $n_s = 1.55$. We stress that, here, the assumption of ideal spherical shape could in principle not be adequate, even if no appreciable differences are expected in the complex amplitude until the shape is approximately isometric (Potenza and Milani 2014). This could be at the origin of the larger spread in the data, as well as of the (slight) disagreement with the expected behavior in the region of the Mie maximum. Moreover, we notice that in this case almost no events are found belonging to the phase inverted region of the plot, thus preventing the analysis previously performed for water droplets about the sign of the swing.

In Fig. 8, we show the results obtained by applying the LUT reported in Fig. 2 to the dataset in Fig. 7. As above, panel a gives diameter-refractive index 2D histogram, panel b the size distribution, and panel c the index distribution. First of all, we notice that particle size distribution has a sudden drop at a radius of about 300 nm, which is in agreement with the expected size-cut (340 nm) of the aerosol generator (1 μm aerodynamic diameter) for NaCl particles (density = 2.16 g/cm^3). It is noteworthy that the refractive index size distribution is broader than in the case of water, probably due to non-spherical shape of salt particles. Statistical analysis of the histogram leads to a refractive index $m = 1.55 \pm 0.2$ which is in agreement with the expected value.

Graphite nanoparticles

We report the results obtained with a sample of graphite nanoparticles produced by a graphite spark aerosol generator by Palas GmbH (Mod. DNP digital 3000), which can be considered a proxy for black carbon (BC). BC is as carbonaceous material with a deep black appearance, which is caused by a significant, non-zero imaginary part of the refractive index that is wavelength independent over the visible and near-visible spectral regions (Moosmüller et al. 2009). The aerosol generator uses a jump spark between two graphite electrodes under high voltage to produce small particles of graphite. Due to the high number concentration of primary graphite particles, they coagulate into agglomerates of larger size, resulting in a polydisperse aerosol population.

Again, in this case the ideal spherical shape cannot be safely assumed, the main limitation likely being the assumptions of the spherical and homogeneous internal structure of the particles. In principle, this would prevent the use of Mie theory. As a consequence, we analyze data through the LUT introduced above, thus limiting our assumptions to isometric-shaped particles with unknown, effective refractive indexes. In Fig. 9, we report the SPES data. The red line represents the result of the

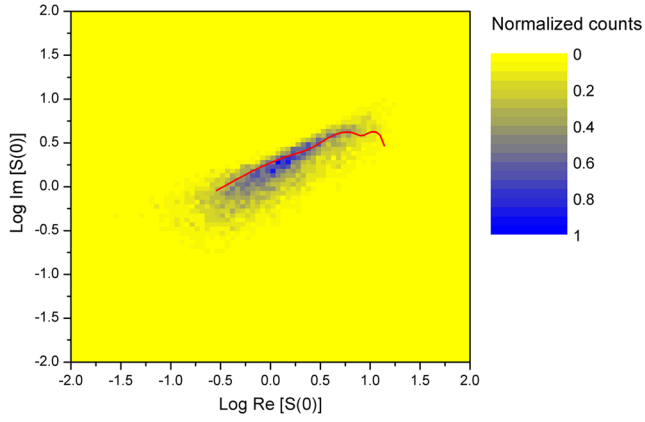

Fig. 7 Experimental results (color histogram) obtained with NaCl particles, compared to the expected values for spheres obtained from the Mie theory (red line)

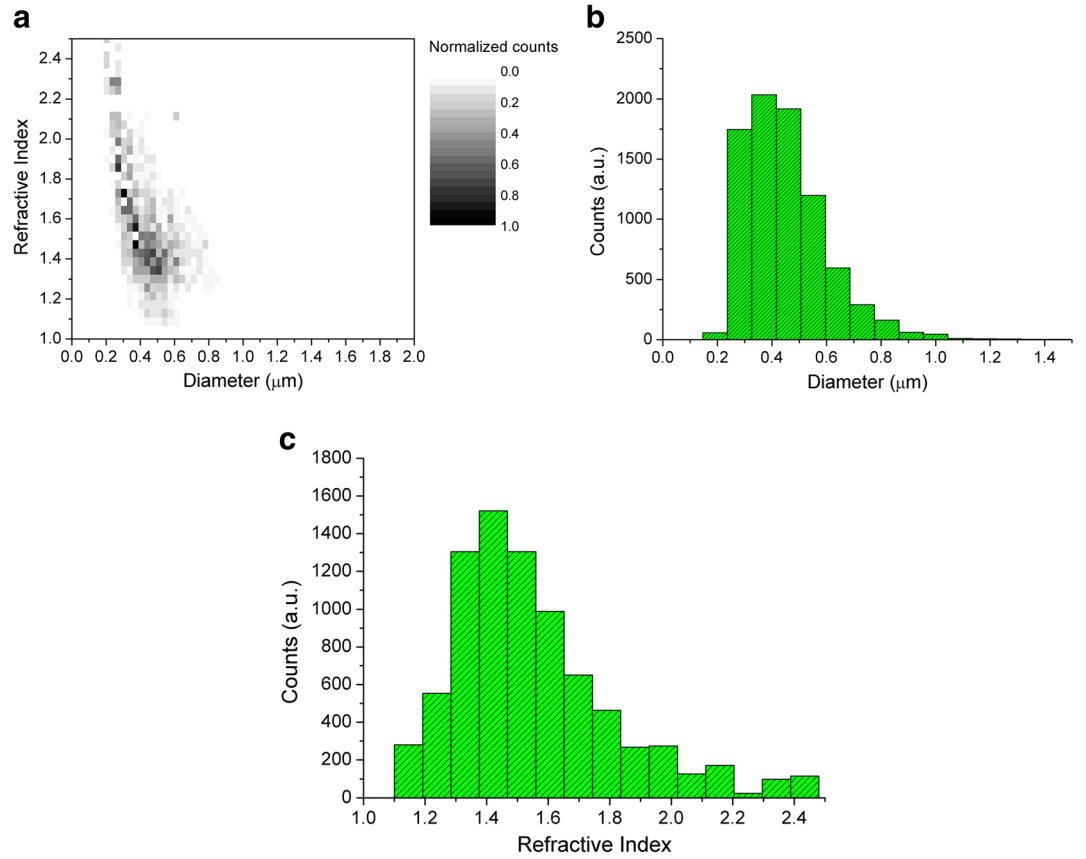

Fig. 8 Sizes and refractive indexes obtained from the data in Fig. 7 (NaCl particles) by means of the LUT represented in Fig. 2. As in Fig. 6, panel **a** represents the 2D histogram, panels **b** and **c** the size and refractive index distributions, respectively

Mie theory evaluated for the best fitted values for both the real and imaginary parts of the refractive index, thus obtaining $n + \mathrm{i}\,k = 1.3 + 0.2\,\mathrm{i}$. The discrepancy visible at the larger sizes (i.e., larger $S(0)$) is discussed below.

We exploited the LUT reported in Fig. 3 ($k = 0.2$, as from the best fit to data) to recover the size and the real part of the refractive index for each particle, as described above. The results are shown in Fig. 10. The size distribution is in accordance with the expectations. The distribution of the real parts of the refractive indices shows a rampant skewness. This is probably due to the heterogeneous internal structure of particles produced through

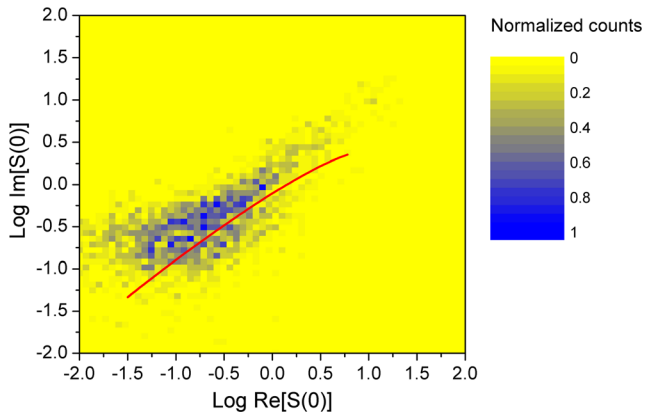

Fig. 9 Experimental results (color histogram) obtained with graphite nanoparticles. The non-compact structure of the graphite nanoparticles makes it impossible to compare to Mie theory. The red line represents the best fitted curve obtained from the Mie theory (see text for discussion)

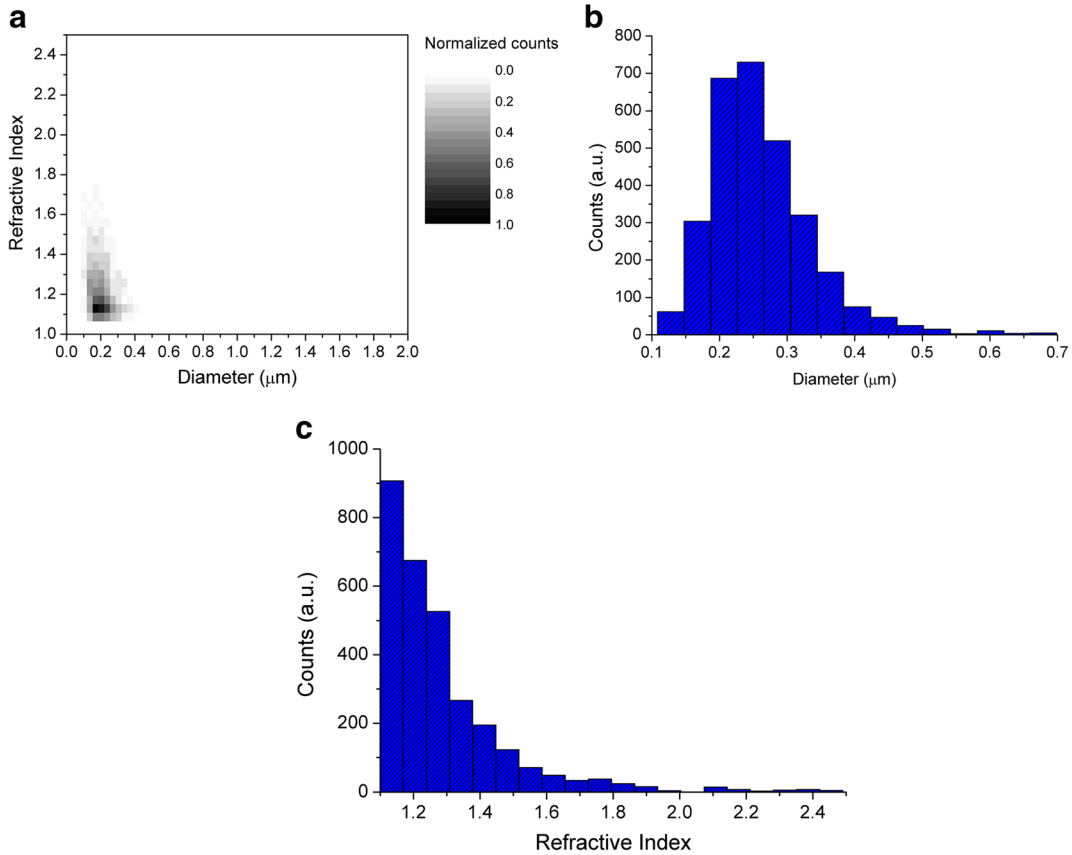

Fig. 10 Sizes and refractive indexes obtained from the data in Fig. 9 (graphite nanoparticles) by means of the LUT represented in Fig. 3. Panel **a** represents the 2D histogram, panels **b** and **c** the size and refractive index distributions, respectively

coagulation of very small graphite particles formed by the graphite spark aerosol generator. Aggregates (likely fractals) have a non-compact internal structure that affects the polarizability of each particle, and therefore the refractive index estimated through the LUT by interpreting data in terms of uniform spheres with an effective refractive index. This can be the reason why the effective refractive index is lower than the one expected for single small spheres of BC—e.g., $n = 1.96 + 0.66$ i at 589 nm (Seinfeld and Pandis 1998).

Here we stress that the complex polarizability of such particles is actually influenced by the specific internal structure. Keeping into account these effects is still an open issue and a very difficult task to be addressed (for an illuminating review, see Sorensen 2001). Nevertheless, data suggest that small and large particles have different structures, as expected on the basis of simple models of the aggregates based on the Maxwell-Garnett approximation for the average polarizability. This shows that larger particles are expected to be endowed with lower polarizabilities than smaller ones due to the fractal nature (Sorensen 2001; Potenza and Milani 2014) as observed in our data where the average size increases of about 15% when we consider refractive indexes $1.1 < n < 1.25$ with respect to the larger values of n (see Fig. 10a). This also explains the visible discrepancy between the red line and the SPES data in Fig. 9.

Pyrethrum smoke

Another test was done measuring smoke particles produced by the combustion of a pyrethrum coil. This type of smoke is far from containing pure black carbon particles, as it was verified by collection of the particles on a PTFE filter and the analysis of the particle deposit absorbance by the multi-wavelength polar photometer PP_UniMI (405, 532, 635, and 780 nm) (Bernardoni et al. 2017; Vecchi et al. 2014). Wavelength dependence

of absorption properties of particles is generally expected to follow a $\lambda^{-\alpha}$ trend (where α is called Ångström absorption coefficient). Whether $\alpha = 1$ is expected for BC particles in the Rayleigh regime (Moosmüller et al. 2009), multi-wavelength measurements of pyrethrum coil smoke showed $\alpha = 5.0 \pm 0.4$. This indicates possible emission of light-absorbing organics (e.g., brown carbon (BrC), HUmic-LIke Substances (HULIS)) from pyrethrum coil combustion. The mass absorption efficiency (MAE) of light-absorbing organic species is much less than the one of BC at longer wavelengths but increasing sharply towards lower wavelengths (Andreae and Gelencsér 2006): as examples, Utry et al. (2013) reported MAE = 0.319 m^2/g and MAE = $2.97 \cdot 10^{-2}$ m^2/g for HULIS at 532 and 375 nm, respectively, with $\alpha = 5.87$; α(BrC) up to 9.5 have been reported in the literature (Lack and Langridge 2013).

The analysis of data collected by SPES immediately shows the presence of absorption by comparison with the data from water and salt. In this case, a value of $k = 0.12$ has been found to be adequate to describe the overall dataset, although differences are evident between the smaller and the larger particles. In particular, smaller particles are characterized by a slightly smaller value of k of the order of 0.10, larger particles by $k = 0.15$. These differences can be neglected at this stage of approximation in the data interpretation, the changes being of the order of less than 20% in the average size. Moreover, Fig. 11 shows that the particles are well described by spherical shapes, as indicated by both the limited extension of the population and the presence of an evident maximum in the values of $S(0)$. The distributions of the size and the real part of the refractive index are shown in Fig. 12.

Discussion and conclusions

We have shown that the novel SPES method operated in air may represent an important advance among the methods for aerosol characterization. Without pretending of being a substitute of existing devices and methods, we are convinced that SPES can represent a novel, precise source of information complementary to that from other instruments.

As we have preliminarily shown with our data, SPES allows to give insight into details of single particles almost inaccessible before, at least with online instrumentation capable of monitoring in continuous large volumes of air and accumulating huge statistics (e.g., OPC). SPES opens the possibility to determine both the particle size and the refractive index in the case of non-absorbing particles. In addition, aerosol populations with size polydispersity and homogeneous composition allow to reach very high precision in the refractive index determination, as we carefully verified with water and salt. For absorbing particles, the imaginary part of the refractive index can be measured once the real part is roughly known.

This is possible thanks to single-particle measurements of untreated samples, allowing to either recover detailed statistical properties of the analyzed population or average properties obtained by integrated measurements. From the experimental point of view, SPES is immune from almost any calibration and the rejection of spurious signals is rigorously implemented through accurate signal analysis

In perspective, operating SPES in cascading with a device for particle size segregation will allow to reduce

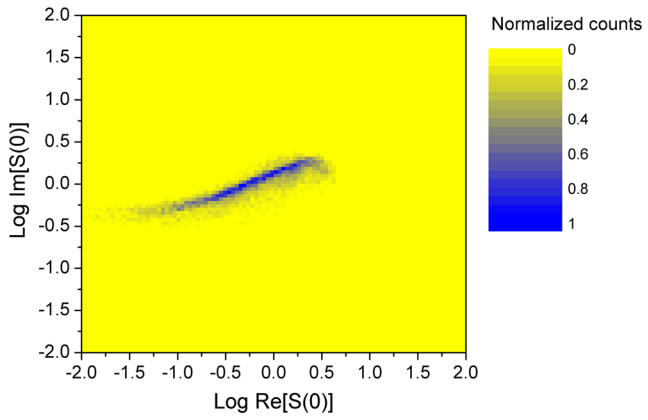

Fig. 11 Experimental results (color histogram) obtained with pyrethrum smoke particles

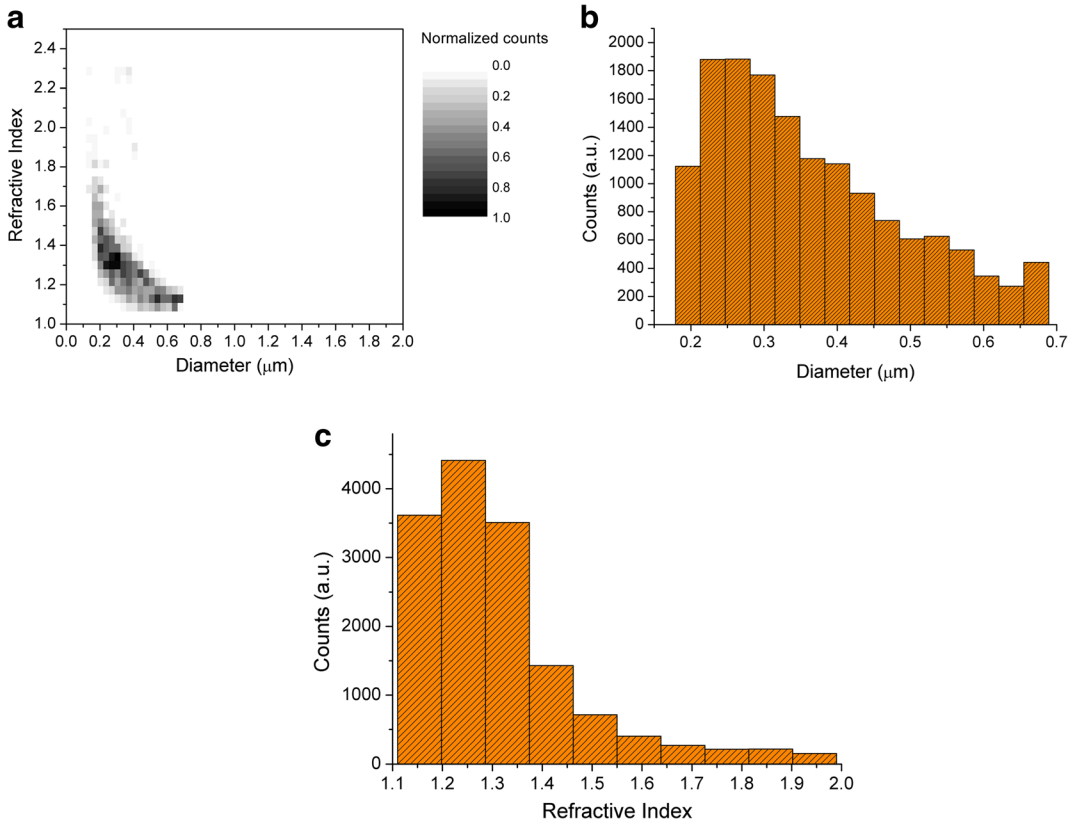

Fig. 12 Sizes and refractive indexes obtained from the data in Fig. 11 (pyrethrum smoke) by means of the LUT obtained for $k = 0.12$. Panel **a** represents the 2D histogram, panels **b** and **c** the size and refractive index distributions, respectively

the number of free parameters to be fitted to data, opening new possibilities for aerosol characterization. As an example, in such a way it could be possible to gain information about non-spherical shape in case of aerosol of homogeneous composition: indeed, thanks to single particle detection, SPES data can be easily compared to results expected for spherical particles population.

Despite these advantages, SPES currently suffers of some drawbacks. First of all, the frequency of the recorded events is limited, thus preventing from very fast and time resolved measurements. This is due to three main issues: (1) the tight focusing rampantly reduces the scattering volume, so that the cross section encountered by the flowing dust particles which generate signals is limited; (2) the signal shape analysis guarantees the superior quality of the data but reduces the number of the validated particles; (3) distributing the events in the 2D complex plane requires a very large number of events to be accumulated in order to really take advantage from the refined analytical approaches described above. Quantitatively speaking (1) in our apparatus we maintained a rate of acquisition of approximately 500 particles/s; (2) among these, about 20% were validated; (3) results are typically spread over several 100 bins. Roughly, 2 min measurement will give about 10^4 events, providing a Poisson statistical error of approximately 10% overall the 2D histogram. The capability of generating a larger amount of information automatically requires to drastically improve the number of recorded events, thus demanding for longer measurement times.

Limitations are also imposed by the laser instabilities that limit the SPES sensitivity and resolution. In our device, a typical peak-to-peak noise of approximately $2{\cdot}10^{-4}$ was present, as mentioned above. By adopting the signal shape analysis, we obtain a corresponding sensibility of approximately 10^{-2} and $3{\cdot}10^{-2}$ for *Re* $S(0)$ and *Im* $S(0)$, respectively. Accurate characterization of the source and a careful choice of the bandwidth have been performed, thus bringing the current device close to an optimum. Therefore, this is not an issue that can be easily circumvented, at least without making huge

efforts in compensating the instabilities. As a result, in order to gauge the sensibility, a change of the focal spot size is the easiest solution that nevertheless implies to modify the instrumentation. In the case of tighter focusing, it also reduces the counting rate as discussed above.

Acknowledgements We acknowledge Marzio Giglio for useful discussions, F. Cavaliere and D. Viganò of the Mechanical Workshop of the Physics Department for supporting the realization of the SPES instrumentation.

Compliance with ethical standards

Conflict of interest The authors declare that they have no conflict of interest.

References

Albani S, Mahowald NM, Perry AT, Scanza RA, Zender CS, Heavens NG, Maggi V, Kok JF, Otto-Bliesner BL (2014) Improved dust representation in the community atmosphere model. J Adv Model Earth Syst 6:541–570. doi:10.1002/2013MS000279

Andreae MO, Gelencsér A (2006) Black carbon or brown carbon? The nature of light-absorbing carbonaceous aerosols. Atmos Chem Phys 6:3131–3148

Bassini A, Menchise M, Musazzi S, Paganini E, Perini U (1997) Interferometric system for precise submicrometer particle sizing. Appl Opt 36:8121–8127

Batchelder JS, Taubenblatt MA (1989) Interferometric detection of forward scattered light from small particles. Appl Phys Lett 55:215–217

Bauer E, Ganopolski A (2014) Sensitivity simulations with direct shortwave radiative forcing by aeolian dust during glacial cycles. Clim Past 10:1333–1348

Bernardoni V, Valli G, Vecchi R (2017) Set-up of a multi wavelength polar photometer for off-line absorption coefficient measurements on 1-h resolved aerosol samples. J Aerosol Sci 107:84–93

Bohren CF, Huffmann DR (1983) Absorption and scattering by small particles. Wiley, New York

Chemyakin E, Burton S, Kolgotin A, Müller D, Hostetler C, Ferrare R (2016) Retrieval of aerosol parameters from multiwavelength lidar: investigation of the underlying inverse mathematical problem. Appl Opt 55:2188–2202

Chylek P, Grams GW, Pinninck RG (1976) Light scattering by irregular randomly oriented particles. Science 193:480–482

Cotterell MI, Mason BJ, Preston TC, Orr-Ewing AJ, Reid JP (2015) Optical extinction efficiency Measurements on fine and accumulation mode aerosol using single particle cavity ring-down spectroscopy. Phys Chem Chem Phys 17:15843–15856. doi:10.1039/C5CP00252D

Cotterell MI, Preston TC, Orr-Ewing AJ, Reid JP (2016) Assessing the accuracy of complex refractive index retrievals from single aerosol particle cavity ring-down spectroscopy. Aerosol Sci Technol 50:1077–1095. doi:10.1080/02786826.2016.1219691

David G, Esat K, Ritsch I, Signorell R (2016) Ultraviolet broadband light scattering for optically-trapped submicron-sized aerosol particles. Phys Chem Chem Phys 18:5477–5485

Harvey LDD (1988) Climatic impact of ice-age aerosols. Nature 334:333–334

Heim M, Mullins BJ, Umhauer H, Kasper G (2008) Performance evaluation of three optical counters with an efficient "multimodal" calibration method. J Aerosol Sci 39:1019–1031

IPCC, 2013: Climate Change 2013: The Physical Science Basis. Contribution of Working Group I to the Fifth Assessment Report of the Intergovernmental Panel on Climate Change [Stocker, T.F., D. Qin, G.-K. Plattner, M. Tignor, S.K. Allen, J. Boschung, A. Nauels, Y. Xia, V. Bex and P.M. Midgley (eds.)]. Cambridge University Press, Cambridge, United Kingdom and New York, NY, USA, 1535 pp, https://doi.org/10.1017/CBO9781107415324

Lack DA, Langridge JM (2013) On the attribution of black and brown carbon light absorption using the Ångström exponent. Atmos Chem Phys 13:10535–10543

Lambert F, Delmonte B, Petit JR, Bigler M, Kaufmann PR, Hutterli MA, Stocker TF, Ruth U, Steffensen JP, Maggi V (2008) Dust-climate couplings over the past 800,000 years from the EPICA Dome C ice core. Nature 452:616–619

Mishchenko MI, Hovenier JW, Travis LD (eds) (1999) Light scattering by nonspherical particles: theory, measurements, and applications. Academic Press, San Diego

Moosmüller H, Chakrabarty RK, Arnott WP (2009) Aerosol light absorption and its measurement: a review. J Quant Spectrosc Radiat Transf 110:844–878

Nakagawa M, Nakayama T, Sasago H, Ueda S, Venables DS, Matsumi Y (2016) Design and characterization of a novel single-particle polar nephelometer. Aerosol Sci Technol 50:392–404

Newton RG (1976) Optical theorem and beyond. Am J Phys 44:639–642

Potenza MA, Sabareesh KP, Carpineti M, Alaimo MD, Giglio M (2010) How to measure the optical thickness of scattering particles from the phase delay of scattered waves: application to turbid samples. Phys Rev Lett 105:193901

Potenza MAC, Milani P (2014) Free nanoparticle characterization by optical scattering field analysis: opportunities and perspectives. J Nanopart Res 16:2680

Potenza MAC, Sanvito T, Pullia A (2015b) Measuring the complex field scattered by single submicron particles. AIP Adv 5:117222

Potenza MAC, Sanvito T, Argentiere S, Cella C, Paroli B, Lenardi C, Milani P (2015a) Single particle optical extinction and scattering allows real time quantitative characterization of drug payload and degradation of polymeric nanoparticles. Sci Rep 5:18228

Potenza MAC, Sanvito T, Pullia A (2015c) Accurate sizing of ceria oxide nanoparticles in slurries by the analysis of the optical forward scattered field. J Nanopart Res 17:110

Potenza MAC, Albani S, Delmonte B, Villa S, Sanvito T, Paroli B, Pullia A, Baccolo G, Mahowald N, Maggi V (2016) Shape and size constraints on dust optical properties from the Dome C ice core, Antarctica. Sci Rep 6:28162

Ruth U (2002) Concentration and size distribution of microparticles in the NGRIP Ice Core (Central Greenland) during the last glacial period. PhD Dissertation at Department of

Geosciences of the University of Bremen. Published as Report n. 428 of the Berichte zur Polar- und Meeresforschung (ISSN 1618-3193). Available at: http://www.ub.uni-heidelberg

Sachweh B, Umhauer H, Ebert F, Buttner H, Friehmelt R (1998) In situ optical particle counter with improved coincidence error correction for number concentrations up to 10^7 particles cm^{-3}. J Aerosol Sci 29:1075–1086

Sanvito T, Zocca F, Pullia A, Potenza MAC (2013) A method for characterizing the stability of light sources. Opt Express 21: 24630–24635

Seinfeld JH, Pandis SN (1998) Atmospheric chemistry and physics. From air pollution to climate change. Wiley, New York

Sorensen CM (2001) Light scattering by fractal aggregates: a review. Aerosol Sci Technol 35:648–687

Taubenblatt MA, Batchelder JS (1991) Measurement of the size and refractive index of a small particle using the complex forward-scattered electromagnetic field. Appl Opt 30:4972–4979

Utry N, Ajtai T, Filep Á, Dániel PM, Hoffer A, Bozoki Z, Szabó G (2013) Mass specific optical absorption coefficient of HULIS aerosol measured by a four-wavelength photoacoustic spectrometer at NIR, VIS and UV wavelengths. Atmos Environ 69:321–324

Van de Hulst HC (1981) Light scattering by small particles. Dover, New York

Vecchi R, Bernardoni V, Paganelli C, Valli G (2014) A filter-based light-absorption measurement with polar photometer: effects of sampling artefacts from organic carbon. J Aerosol Sci 70: 15–25

Villa S, Sanvito T, Paroli B, Pullia A, Delmonte B, Potenza MAC (2016) Measuring shape and size of micrometric particles from the analysis of the forward scattered field. J Appl Phys 119:224901

Zarzana KJ, Cappa CD, Tolbert MA (2014) Sensitivity of aerosol refractive index retrievals using optical spectroscopy. Aerosol Sci Technol 48:1133–1144